Insights into Ionic Liquid Electrolyte Transport and Structure via Operando Raman Microspectroscopy

Jack Fawdon,[†] Gregory J. Rees,[†,‡] Fabio La Mantia,[¶] and Mauro Pasta[*,†,‡]

†*Department of Materials, University of Oxford, Parks Rd, Oxford, OX1 3PH, U.K.*

‡*The Faraday Institution Quad One, Harwell Science and Innovation Campus, Didcot, U.K.*

¶*Universtät Bremen, Energiespeicher-und Energiewandlersysteme, Bibliotechkstraße 1, Bremen, 28359, Germany*

E-mail: mauro.pasta@materials.ox.ac.uk

Abstract

Ionic liquid electrolytes (ILEs) have become popular in various advanced Li-ion battery chemistries because of their high electrochemical and thermal stability, and low volatility. However, due to their relatively high viscosity and poor Li^+ diffusion, it is thought large concentration gradients form, reducing their rate capability. Here, we utilised operando Raman microspectroscopy to visualise ILE concentration gradients for the first time. Specifically, using lithium bis(fluorosulfonyl)imide (LiFSI) in N-propyl-N-methylpyrrolidinium FSI, its "apparent" diffusion coefficient, lithium transference number, thermodynamic factor, ionic conductivity and resistance of charge-transfer against lithium metal, were isolated. Furthermore, the analysis of these concentration gradients led to insights into the bulk structure of ILEs, which we propose is composed of large, ordered aggregates.

1

As lithium-ion batteries (LIBs) approach their theoretical energy limit, high energy alternatives are required for the increasingly high energy applications society now depends on. Popular strategies to improve energy density include utilising high-voltage cathodes,[1] conversion cathodes[2] or lithium metal anodes.[3] Conventional electrolyte compositions used in LIBs, such as 1 M LiPF$_6$ in EC:DMC (1:1 v/v), have proven to be unsuitable due to the unfavourable solid (or cathodic) electrolyte interphase (SEI or CEI) that forms.[4] In recent years, researchers have shown that using ionic liquid electrolytes (ILEs) improves the cyclability because of the stable SEI/CEI on the respective electrode surface.[5–7] However, with multiple ions in solution and an often high viscosity, ILEs exhibit particularly poor transport properties.[8,9] This limits their rate performance, as ohmic resistance and concentration gradient formation lead to increasing overpotential with increasing current density. Furthermore, in lithium metal batteries (LMBs), the depletion of Li$^+$ at the lithium metal surface has been proven to induce lithium dendrite growth and short-circuiting.[10]

Common ILEs used for battery applications contain 3 or 4 ions, and due to D_{Li^+} often being the lowest, the transference number of Li$^+$ (t_{Li^+}) in ILEs has shown to be very low.[11] Concentration gradients form when $t_{Li^+} \neq 1$, and become increasingly steep as t_{Li^+} and D_{app} decrease. Recently, the most popular method for determining t_{Li^+} in ILEs is via (electrophoretic) pulsed-field gradient nuclear magnetic resonance (pfg-(e)NMR) studies, where self-diffusion coefficients of all the ions in solution are measured and t_{Li^+} is subsequently calculated. These studies have shown $t_{Li^+} < 0.1$. Intriguingly, using eNMR, Gouverneur et al. showed t_{Li^+} is negative for LiTFSI in EmimTFSI solution implying Li$^+$ was moving in the "wrong direction".[12,13] Others have measured t_{Li^+} using electrochemical impedance spectroscopy (EIS) and monitoring the finite-length Warburg diffusion resistance (W_d).[14,15] However, this method includes an electrolyte ideality assumption, which is especially problematic in a concentrated electrolyte or ILE.[16] Although these techniques have shed light on the complexities and intricacies of ILEs transport, there is yet to be a complete experimental study that monitors both D_{app} and t_{Li^+}, with an added thermodynamic understanding

through χ_M.

For a comprehensive understanding of binary electrolyte transport, researchers have utilised operando magnetic resonance imagining (MRI) and Raman techniques to visualise concentration gradients.[17–20] These studies have not yet been extended to ternary systems or ionic liquid systems. Here, we use operando Raman microspectroscopy to measure Li^+ concentration gradients in an IL-based electrolyte system. We focus on 0.5 m, 1 m and 2 m LiFSI in $Pyr_{1,3}FSI$, a common electrolyte system used in high-energy cells.[5,6,21] By studying the concentration gradients we gained valuable information on intermolecular structure and the potential mechanism of ion-transport. Concentration gradient formation is regarded as ILEs' primary weakness in LIB and LMBs, so the visualisation of the gradient is of particular importance for the understanding and progression of ILEs.
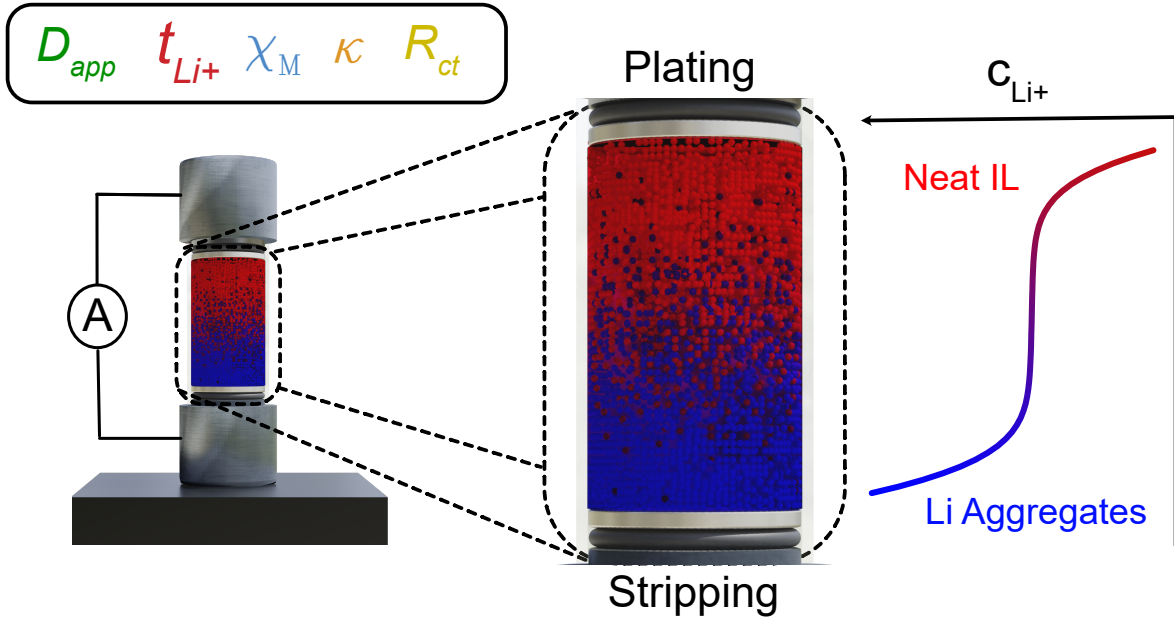

Figure 1: **Method for visualising ILE concentration profile and obtaining D_{app}, t_{Li^+}, χ_M, κ and R_{ct} values.** The asymmetry in the concentration gradient is a result of accumulation of Li^+ species at the bottom of cell.

Concentration Gradient Visualisation. The general method for concentration gradient visualisation using operando Raman microspectroscopy (Figure 1) has been illustrated in our previous work;[18] specifically a time-series of one-dimensional (1D) Raman scans across

a custom-built optical Li|Li symmetric cell while current is passed. Importantly, the cell was placed vertically on the stage, with stripping occurring at the bottom and plating at the top, to avoid natural convection from density differences of the bulk concentration. The line-scan was performed every 4 hours for 36 hours. Electrolyte solutions were prepared gravimetrically (molal) to increase reliability and accuracy of preparation; for density measurements, and molarity equivalents see Supporting Methods 2.

Due to there being no solvent peak to normalise the FSI^- and $Pyr_{1,3}^+$ peak area, an alternative method for equating each point scan to c_{Li^+} was required. We opted for a correlation of c_{Li^+} to the 730 cm^{-1} FSI^- peak shift. Representing the S-N-S bending mode,[22] the 730 cm^{-1} peak shifts to higher wavenumbers monotonically with increasing c_{Li^+} due to the continuing formation of high-energy bonding in $Li(FSI)_2^-$ structures.[23] Figure 2a shows the non-linearity of wavenumber increase with c_{Li^+} as the LiFSI concentration approaches saturation. An alternative method involved using area ratios FSI^- 730 cm^{-1} and $Pyr_{1,3}^+$ 900 cm^{-1} peaks. Due to the increased spectral noise using this method, we selected the former method; further analysis is shown in Supporting Discussion 1.
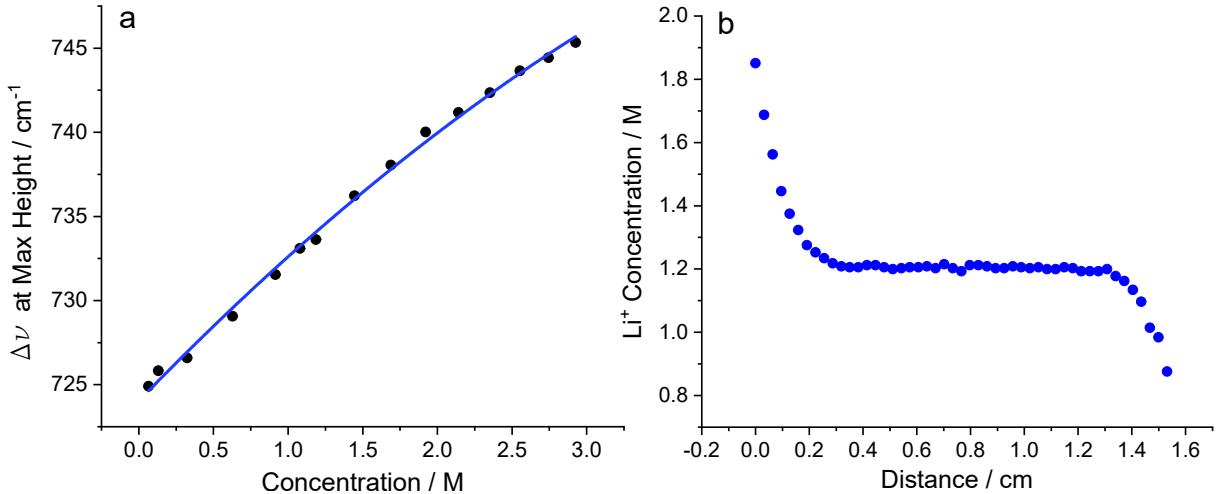

Figure 2: **Method for isolating ILE concentration profile:** a) $\sim$730 cm^{-1} FSI^- S-N-S peak shifts to higher wavenumber with Li$^+$ concentration. b) Concentration profile of $Li + of 1mLiFSI in Pyr_{1,3}FSI$, at 100 μA cm^{-2} after 12 hours.

Using the 730 cm^{-1} peak shift method, we checked the mass-balance of the system by

integrating each concentration profile over the 36 hour experiment, and noted no change with each integral being within 1.2 % of the highest and lowest profile integral. We therefore concluded this is a valid method for calibrating concentration in ILEs.

Asymmetry and Structural Implications. Figure 2b shows a concentration profile of Li^+ in 1 m LiFSI in $Pyr_{1,3}$FSI at 100 μA cm^{-2} after 12 hours. Surprisingly, the profile had an asymmetry, with both bulk concentration change and dc/dz being larger on the stripping side compared to the plating side. This seemed unique to ILEs systems, with our previously investigated system, LiFSI in tetraglyme (G4), not showing this phenomenon.[18]

Prior to applying current, the cell rested for 4 hours and a line-scan was recorded. We noticed an increase in concentration at the bottom of the cell, which indicated an accumulation of c_{Li^+} before any current was applied, see Figure 3a. This accumulation suggested distinct Li^+-containing species of higher density were falling due to gravity. To investigate this further, we measured the open circuit voltage (OCV) of the cell while changing the cell's orientation. Figure 3b shows how the OCV changed with time, labelled with the orientation of the cell. It was clear that OCV was dependent on the position of cell, with the potential difference agreeing well with the concentration difference; from the Nernst equation. As shown in Supporting Figure 3, we also saw this phenomena with stainless-steel blocking electrodes, albeit to a lesser extent. This suggested that the reactive electrodes increased bulk flow, perhaps due to volume changes caused by the interfacial reaction.[24]

Several molecular dynamic (MD) studies have proposed the formation of long-range ordered structures in ILEs, with some suggesting mesoscopic aggregate formation.[25,26] Past experimental studies using small angle X-ray scattering (SAXS) experiments have also predicted the formation of mesoscopic aggregates or domains in neat ILs, and with lithium salt in IL solutions.[27–29] NMR measurements have shown similar results.[30] However, there is little consensus on the overall size and structure of the aggregates present in IL and Li-salt solutions. Using Stokes' Law[31] we estimated the size of aggregates to be 3-8 μm; larger than others hypothesised. See Supporting Discussion 2 for further discussion. Further studies are
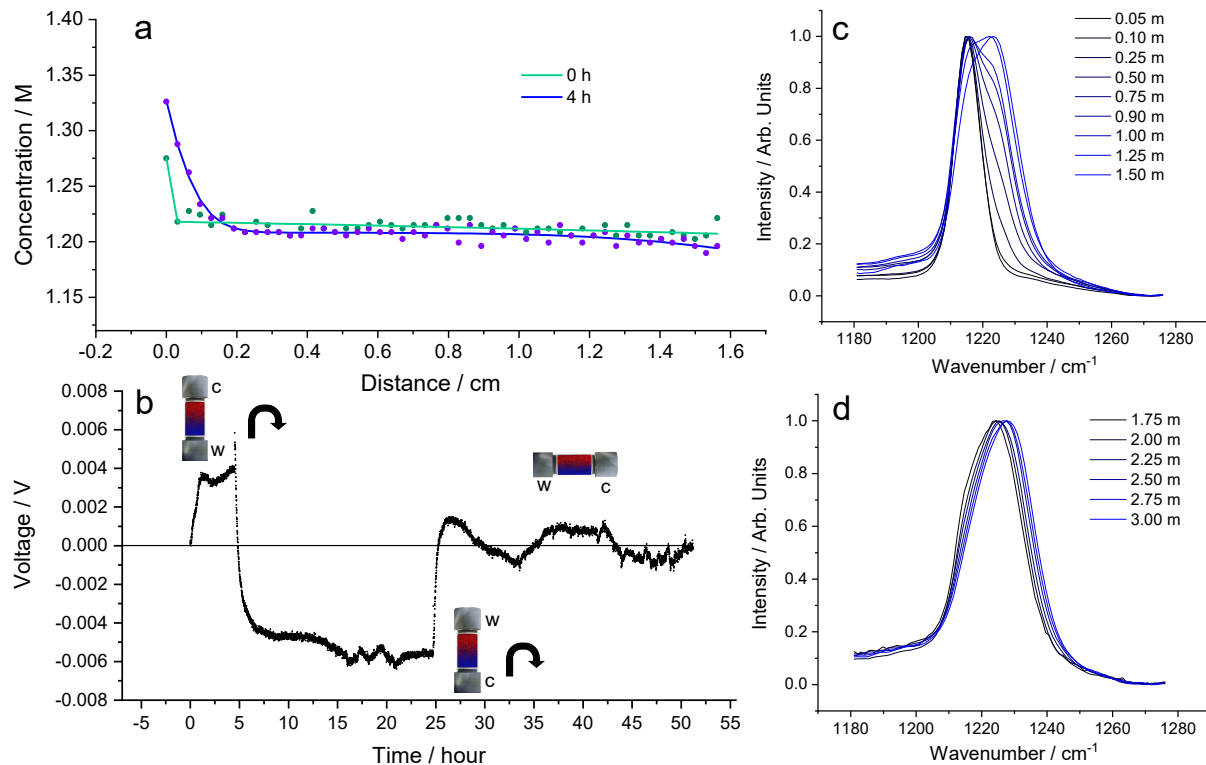
Figure 3: **Asymmetric Concentration Gradients:** a) Formation of concentration differences over 4 h, 0 cm is the bottom of the cell. b) OCV vs. time while no current is passed, showing how orientation affects the OCV of the cell. c) Raman spectra of 0.05 m to 1.5 m showing two distinct FSI$^-$ Raman bands, representing "free" and "bound" FSI. d) Raman spectra from 1.75 m to 3 m showing a peak shift. At ~1.1 m [FSI$^-$]<[Li(FSI)$_2$]$^-$, which was when the 1225 cm^{-1} became more broad.

required however to confirm this value.

The Raman spectra required for c_{Li^+} calibration provided information on electrolyte structural changes with increasing LiFSI content. The peak at 1200-1240 cm^{-1} represents the S=O stretching mode of FSI$^-$. In the neat IL there was a single peak at 1215 cm^{-1} and with increasing LiFSI addition a new, defined peak appeared at 1225 cm^{-1} (Figure 3c). The 1215 cm^{-1} shift ν(S-O) was seen in LiFSI in organic solvents (e.g. LiFSI in G4[18]), but a defined 1225 cm^{-1} peak was unique to ILEs.[23,32] This suggested the ILEs have distinctive structures or domains present that are not in organic-based electrolytes. As has been mentioned in other works, the 1215 cm^{-1} peak was speculated to be free FSI$^-$ and 1225 cm^{-1} was thought to be a bound Li-FSI$_n$ species. The solvation number of the Li$^+$ can be calculated, as shown

in the Supporting Discussion 4, and we concluded it remained constant at 2 (i.e. Li^+ is solvated by two FSI^-, $[Li(FSI)_2]^-$). With FSI^- experiencing two separate environments, it is at $\sim$1.1 m that $[FSI^-] < [Li(FSI)_2]^-$. As the concentration increased past 1.25 m, the 1225 cm^{-1} peak became less defined and more broad (Figure 3d), which we speculate could be due to the fusing of the $[Li(FSI)_2]^-$-derived aggregates forming a homogeneous, percolating network. Indeed, McEldrew et al. predict using MD simulations a "critical threshold" or gelation point where these extended networks form.[33] We propose both the finite aggregates and percolating network are of a higher density than the IL medium that surrounds them.

Li^+ Transport Properties. The 1 m electrolyte was used as a model system to describe the process of fitting and transport property isolation. Equation 1 is a solution to the diffusion equation in a symmetric cell setup, using the interfacial concentration gradient as a spatial boundary condition.[34,35] Each gradient was fitted to this equation, elucidating information on the transport properties of the electrolytes. Due to the gradients' asymmetry, each side of the cell was fitted separately with different diffusion length and interfacial gradient values, with p and s indicating the plating and stripping sides respectively:

$$c_{Li^+}(z,t) = c_{Li^+}^* + a(s)\left\{ \left(\frac{b(s)}{\pi^{\frac{1}{2}}}\right) \exp\left(-\frac{z}{b}\right)^2 - z\,\mathrm{erfc}\left(\frac{z}{b(s)}\right) \right\} - $$
$$c(p)\left\{ \left(\frac{d(p)}{\pi^{\frac{1}{2}}}\right) \exp\left(-\frac{(-z+L)}{d(p)}\right)^2 + (-z+L)\,\mathrm{erfc}\left(\frac{-z+L}{d(p)}\right) \right\} \tag{1}$$

$$a, c\left(= \frac{\mathrm{d}c_{Li^+}}{\mathrm{d}z}\bigg|_{z=0,L} \right) = \frac{J(1 - t_{Li^+})}{nFD_{app}} \tag{2}$$

$$b, d(= L_d) = 2(D_{app(s,p)}t)^{\frac{1}{2}} \tag{3}$$

Figure 4a shows c_{Li^+} gradients of the 1 m electrolyte at different times. As expected, the gradients were large across the electrolyte, with the stripping electrode showing a significant interfacial concentration $(dc/dz_{z=0})$ gradient of $5.30 \pm 0.16 \times 10^6$ mol m^{-4} at 100 μA cm^{-2}. We also performed the measurement at 50 μA cm^{-2} showing $dc/dz_{z=0}$ as $2.78 \pm 0.11 \times 10^6$

mol m^{-4}. As is expected, $dc/dz_{z=0}$ was directly proportional to the current applied, with $dc/dz_{z=0}$ being almost exactly double when a 100 μA cm^{-2} was applied compared to 50 μA cm^{-2}. The plating interfacial gradient ($dc/dz_{z=L}$) at 100 μA cm^{-2} was lower at $3.51 \pm 0.63 \times 10^6$ mol m^{-4}; presumably due to the accumulated aggregates at the bottom of the cell. For comparison, 1 m LiFSI in G4 showed an $dc/dz_{z=0,L}$ as $\sim 1 \times 10^6$ mol m^{-4} at 100 μA cm^{-2}.[18]
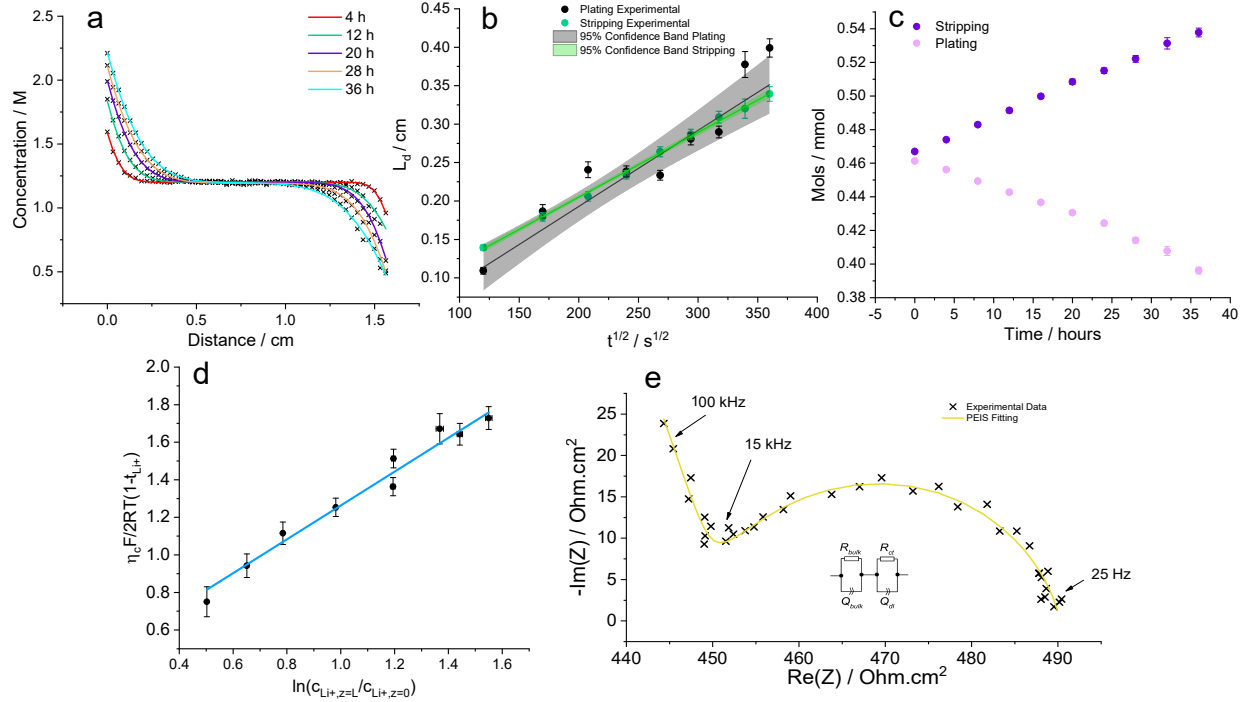

Figure 4: **Concentration gradients and the extraction of 1 m LiFSI in Pyr$_{1,3}$FSI electrolyte properties** a) Li$^+$ concentration gradient formation over time, up to 36 hours with 8 hours gaps. b) Evolution of diffusion length (L_d) with time on the stripping and plating side. c) Change in the molar content on the stripping and plating side of the cell with time. d) Plotting equation 12, illustrating how the η_c function changes linearly with respect to the natural log of concentration ratio of each cell extreme. e) PEIS of electrolyte prior to application of current, indicating a low R_{ct} and R_{bulk}

Diffusion. By monitoring the diffusion length (b and d) over time, one can calculate the "apparent" diffusion coefficient (D_{app}) on both sides of the cell. Figure 4b shows b and d vs. time$^{1/2}$, with the slope being proportional to the D_{app}. Also plotted is the 95% confidence band, which highlights the uncertainty especially on the plating side of the cell. The fitting on the stripping side is much more accurate, which is reflected in the error of the D_{app}

calculation. On the stripping side, $D_{app} = 1.77 \pm 0.064 \times 10^{-11}$ m^{2}s^{-1}, and on the plating side $D_{app} = 2.45 \pm 0.49 \times 10^{-11}$ m^{2}s^{-1}, with a inverse-variance weighted average of 1.78 $\pm 0.09 \times 10^{-11}$ m^{2}s^{-1}. Pulsed field gradient (pfg)-NMR measurements were performed to compare against these values: using the harmonic mean, D_{app} was calculated as 1.77×10^{-11} m^{2}s^{-1} (see Supporting Discussion 2.5), very similar to D_{app} calculated using concentration visualisation.

Transference Number. The transference number of Li$^+$ (t_{Li+}) was calculated from the fitted concentration gradient. Conventionally, t_{Li+} is measured via the Hittorf method, which looks at calculating the change in concentration on either the plating or stripping side of the cell after a known amount of current is passed.[34] This was particularly straightforward when utilising concentration gradient visualisation techniques, as one can monitor the concentration on each side of the cell by integrating under the concentration curve. Moreover, those using a conventional Hittorf setup would not notice the initial gradient from the settling aggregates. To the best of our knowledge, the Hittorf method has not been utilised for studying t_{Li+} in lithium-ion room temperature ILEs, with the majority of groups using pfg-NMR or eNMR, and others describing "ionic melts".[36–40] Like Gouverneur, who used eNMR, we used an "external" reference, namely the centre-of-mass reference. t_{Li+} was calculated:

$$t_{Li+} = 1 - \frac{\Delta n_{Li+}}{n_{charge}} = \frac{A \cdot F(\Delta \int_0^{z_{cell}/2} c_{Li+} dz)}{Q} \tag{4}$$

$$\Delta c_{Li+} = c_{Li+}^{0h} - c_{Li+}^{t} \tag{5}$$

Where n_{charge} is the number of moles of charge passed, Δn_{Li+} is the molar difference between the two sides of the cell before and after time, t, Q is the charge passed over time, and A is the area of the electrode.

Figure 4c shows how the concentration changed for the stripping and plating side; note

the change in area is linear indicating the movement of the aggregated structures remained constant, and so did t_{Li+}. Using the initial concentration profile prior to application of current, t_{Li+} was calculated for each scan over time, and the average t_{Li+} was calculated from the inverse-variance weighted mean. On the stripping side t_{Li+} was calculated as -0.088 ± 0.024 and on the plating side, 0.114 ± 0.062, with a weighted average of -0.062 ± 0.070. Again, the lower value on the stripping side was likely due the accumulation of higher density aggregates on oxidation of Li.

By using the pfg-NMR diffusivities and measured concentrations, t_{Li+} via pfg-NMR was 0.0941, but without an electric field (like in eNMR), migration was not taken into account.

Thermodynamic Factor. The molar thermodynamic factor (χ_M) correlates the electrolytes' thermodynamic activity with concentration.[41] To our knowledge, no room-temperature Li-ion ILEs' χ_M has been reported, but the activity of various $LiNO_3$-$AgNO_3$ melt compositions have been measured by Richter a few decades ago, for comparison.[42] χ_M was calculated:

$$\chi_M = 1 + \frac{\ln f_\pm}{\ln c} = \frac{F}{2RT(1 - t_{Li+})} \frac{d\eta_c}{d\ln \frac{c_{Li+,z=L}}{c_{Li+,z=0}}} \tag{6}$$

Where $f_\pm$ is molar activity coefficient. Using the PEIS data prior to each line scan, η_c was calculated by $\eta_c = \eta_{total} - I(R_{bulk} + R_{ct})$, where η_{total} is measured from the chronopotentiometry data and the resistances are from PEIS. χ_M was measured as 0.906 ± 0.064 (Figure 4d), which is reasonable if one were to compare against Richter's findings.

Ionic Conductivity and Resistance of Charge-Transfer. From PEIS, prior to current being passed we can measure the ionic conductivity (κ) and resistance of charge-transfer (R_{ct}) (Figure 4e). κ was calculated as 3.52 ± 0.011 mS cm^{-1}, which agreed well with previous literature values. Using the pfg-NMR data the Haven ratio was calculated as 0.520, showing a significant amount of ion-ion correlation. R_{ct} was calculated as 44.3 ± 4.1 $\Omega \cdot$ cm^2, assumed to be a combination of classical charge-transfer and SEI resistance. ILEs containing FSI$^-$ in particular have shown to have fast charge-transfer kinetics, illustrated by their low R_{ct} value.[43,44]

Dependence on Concentration. To understand transport changes with a varying amount of Li$^+$ present, we performed operando Raman experiments on two other ILE concentrations, namely 0.5 m and 2 m. Like the measurements performed with the 1 m electrolyte, 100 μA cm^{-2} was applied. With the 0.5 m, we also performed a measurement at 50 μA cm^{-2} because at the higher current c_{Li+} dropped very quickly at the plating side. Each D_{app} and t_{Li+} value can be compared to the pfg-NMR values in Table 1.

Table 1: pfg-NMR diffusivities and transference in 0.5 m, 1 m and 2 m at 25 ^{o}C

$\mathbf{c}_{Li}{}^+$ / M	$\mathbf{c}_{FSI}{}^-$ / M	$\mathbf{c}_{Pyr}{}^+$ / M	$\mathbf{D}_{Li+}$ x 10^{-11} m^{2}s^{-1}	$\mathbf{D}_{FSI-}$ x 10^{-11} m^{2}s^{-1}	$\mathbf{D}_{Pyr+}$ x 10^{-11} m^{2}s^{-1}	$\mathbf{D}_{app}$ x 10^{-11} m^{2}s^{-1}	$\mathbf{t}_{Li+}$
0.62	4.38	4.08	2.04	2.79	2.47	2.58	0.053
1.19	5.06	3.87	1.42	1.88	1.76	1.77	0.094
2.14	5.63	3.46	0.81	0.97	0.92	0.92	0.169

Figure 5 shows how electrolyte transport and thermodynamic properties were affected by concentration. D_{app}, t_{Li+} and $dc/dz_{z=0,L}$ were taken from the inverse-variance weighted average of the stripping and plating side. Most strikingly, 0.5 m ILE showed many similar transport and thermodynamic values to 1 m. For instance, 0.5 m showed $dc/dz_{z=0,L}$ equal to $\sim$5.5 $\times$ 10^6 mol m^{-4} like 1 m. t_{Li+} for both these concentrations was very low, although due to the error involved it is difficult to report whether the values were negative or positive. Values of χ_M were lower than 1 for both 0.5 m and 1 m, indicating their activity is lower than their concentration due to a high amount of association.

For 2 m, there was a noticeable change in many of the transport and thermodynamic properties. For example, there was a marginal increase in $dc/dz_{z=0,L}$ from $\sim$5.5 to $\sim$6.5 $\times$ 10^6 mol m^{-4}, due to changes of D_{app} and/or t_{Li+}. There was a drop in D_{app} vs. 1 m and 0.5 m. Most certainly there was an increase in t_{Li+}, which indicated a structural change; perhaps correlated to the broadening of the 1200-1240 cm^{-1} peak. An increase χ_M at high concentrations is common amongst electrolyte solutions and is noticeable here too. Furthermore, results from Richter showed similar behaviour. We speculate that as more LiFSI was added there were fewer free FSI$^-$ to stabilise Li$^+$ via extended [Li(FSI)$_2$]$^-$ structures; χ_M then be-
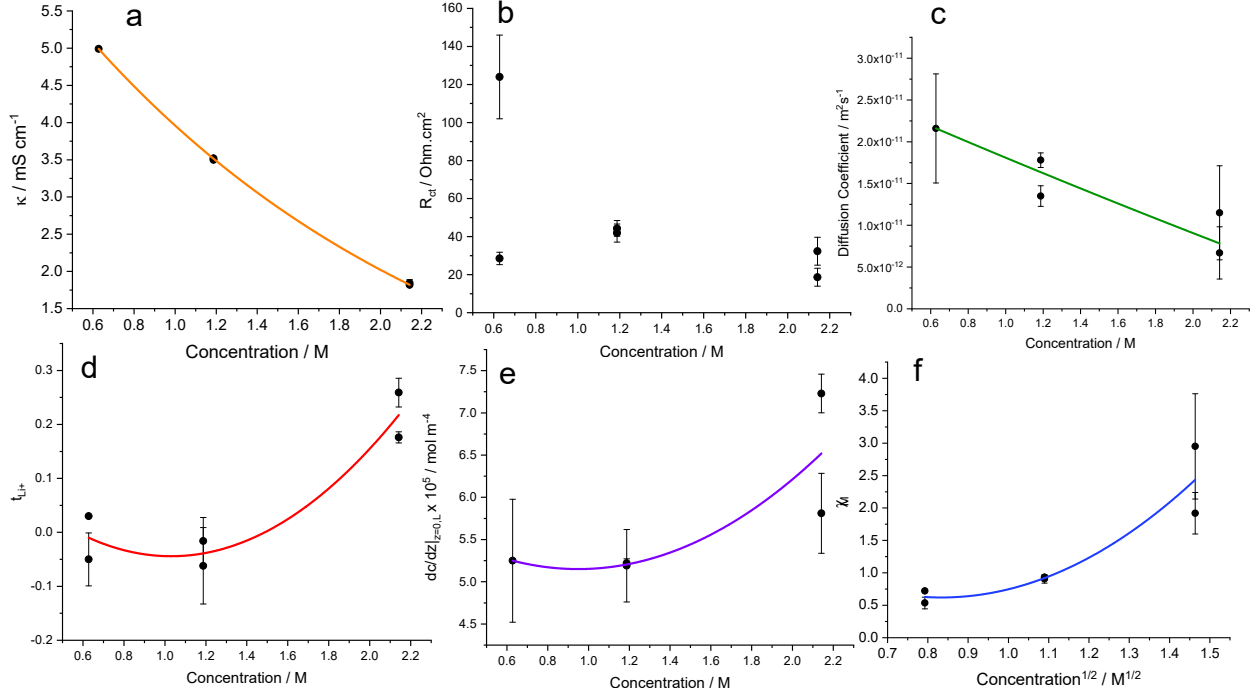
Figure 5: **LiFSI in Pyr$_{1,3}$FSI concentration-dependent transport and thermodynamic properties:** a) Ionic conductivity (κ), fitted by exponential decay. b) Resistance of charge transfer (R_{ct}) showing a marginal increase at 1 m, then a decrease again at 2 m. c) Fickian diffusion coefficient (D_{app}), show a change moving from 1 m to 2 m d) Transference number of lithium (t_{Li^+}), initially very low but showing a marked increase from 1 m to 2 m. e) $(dc/dz)_{z=0}$ at 100 μA cm^{-2}, which was initially constant but showed an increasing moving to 2 m. f) χ_M showing values below 1 for concentrations below 1 m, but increased to $\sim$ 2.5 at 2 m. Values below 1 indicate increased association between Li$^+$ and FSI$^-$ and values above 1 indicate the decreasing amount of free FSI$^-$ present and so an increase in "effective concentration" of Li$^+$.

gan to rise. There was no noticeable trend in R_{ct}, with a clear anomaly for one of the 0.5 m samples, which did not appear to affect the other bulk electrolyte property values described.

This reported data suggested there was a transport mechanism change moving from 1 m to 2 m. We also speculated above that between these concentrations there was a structural change, illustrated from the Raman data. We speculate that when [Li(FSI)$_2$]$^-$ > (FSI)$^-$, ordered networks form, increasing t_{Li^+}.

In summary, by combining spectroscopic and electrochemical techniques with concentration visualisation we have presented particularly valuable findings not yet reported in the ILE literature. With ILEs' main weakness being their transport properties, understanding fully

the origin of this is paramount for their continuing development. We anticipate this work to further promote concentration visualisation's unique ability to fully understand electrolyte properties; and specifically we hope our findings regarding ILE property and structure will inform their ongoing progress.

Acknowledgement

Supporting Information Available

The following files are available free of charge.

1. Supporting Methods: Experimental setup and densitometry measurements.

2. Supporting Discussion: Comparison between calibration methods, estimation of aggregate size with Stokes' Law, description of gradient formation with blocking electrodes, solvation number calculation of Li^+ using Raman, description of D_{app} calculation using pfg-NMR

References

(1) Li, W.; Song, B.; Manthiram, A. High-voltage positive electrode materials for lithium-ion batteries. *Chem. Soc. Rev.* **2017**, *46*, 3006–3059.

(2) Wu, F.; Yushin, G. Conversion cathodes for rechargeable lithium and lithium-ion batteries. *Energy Environ. Sci.* **2017**, *10*, 435–459.

(3) Yoon, H.; Howlett, P. C.; Best, A. S.; Forsyth, M.; MacFarlane, D. R. Fast Charge/Discharge of Li Metal Batteries Using an Ionic Liquid Electrolyte. *J. Electrochem. Soc.* **2013**, *160*, A1629–A1637.

(4) Li, M.; Wang, C.; Chen, Z.; Xu, K.; Lu, J. New Concepts in Electrolytes. *Chem. Rev.* **2020**, *120*, 6783–6819.

(5) Lee, H. J.; Brown, Z.; Zhao, Y.; Fawdon, J.; Song, W.; Lee, J. H.; Ihli, J.; Pasta, M. Ordered LiNi0.5Mn1.5O4 Cathode in Bis(fluorosulfonyl)imide-Based Ionic Liquid Electrolyte: Importance of the Cathode-Electrolyte Interphase. *Chem. Mater.* **2021**, *33*, 1238–1248.

(6) Xiao, A. W.; Lee, H. J. H.-W. W.; Capone, I.; Robertson, A.; Wi, T.-U. U.; Fawdon, J.; Wheeler, S.; Lee, H. J. H.-W. W.; Grobert, N.; Pasta, M. Understanding the conversion mechanism and performance of monodisperse FeF2 nanocrystal cathodes. *Nat. Mater.* **2020**, *19*, 644–654.

(7) Basile, A.; Bhatt, A. I.; O'Mullane, A. P. Stabilizing lithium metal using ionic liquids for long-lived batteries. *Nat. Commun.* **2016**, *7*, 11794.

(8) Watanabe, M.; Thomas, M. L.; Zhang, S.; Ueno, K.; Yasuda, T.; Dokko, K. Application of Ionic Liquids to Energy Storage and Conversion Materials and Devices. *Chem. Rev.* **2017**, *117*, 7190–7239.

(9) Macfarlane, D. R.; Tachikawa, N.; Forsyth, M.; Pringle, J. M.; Howlett, P. C.; Elliott, G. D.; Davis, J. H.; Watanabe, M.; Simon, P.; Angell, C. A. Energy applications of ionic liquids. *Energy Environ. Sci.* **2014**, *7*, 232–250.

(10) Zheng, J.; Kim, M. S.; Tu, Z.; Choudhury, S.; Tang, T.; Archer, L. A. Regulating electrodeposition morphology of lithium: towards commercially relevant secondary Li metal batteries. *Chem. Soc. Rev.* **2020**, *49*, 2701–2750.

(11) Liu, K.; Wang, Z.; Shi, L.; Jungsuttiwong, S.; Yuan, S. Ionic liquids for high performance lithium metal batteries. *J. Energy Chem.* **2021**, *59*, 320–333.

(12) Gouverneur, M.; Schmidt, F.; Schönhoff, M. Negative effective Li transference numbers in Li salt/ionic liquid mixtures: does Li drift in the "Wrong" direction? *Phys. Chem. Chem. Phys.* **2018**, *20*, 7470–7478.

(13) Schönhoff, M.; Cramer, C.; Schmidt, F. Reply to the 'Comment on "negative effective Li transference numbers in Li salt/ionic liquid mixtures: Does Li drift in the "wrong" direction?"' by M. Gouverneur, F. Schmidt and M. Schönhoff,: Phys. Chem. Chem. Phys., 2018, 20, 7470. *Phys. Chem. Chem. Phys.* **2018**, *20*, 30041–30045.

(14) Wohde, F.; Balabajew, M.; Roling, B. Li^{+} Transference Numbers in Liquid Electrolytes Obtained by Very-Low-Frequency Impedance Spectroscopy at Variable Electrode Distances. *J. Electrochem. Soc.* **2016**, *163*, A714–A721.

(15) Scrosati, B.; Croce, F.; Persi, L. Impedance Spectroscopy Study of PEO-Based Nanocomposite Polymer Electrolytes. *J. Electrochem. Soc.* **2000**, *147*, 1718.

(16) Ravn Sørensen, P.; Jacobsen, T. Conductivity, charge transfer and transport number-an ac-investigation of the polymer electrolyte LiSCN-poly(ethyleneoxide). *Electrochim. Acta* **1982**, *27*, 1671–1675.

(17) Bazak, J. D.; Soc, J. E.; Bazak, J. D.; Allen, J. P.; Krachkovskiy, S. A.; Goward, G. R. Mapping of Lithium-Ion Battery Electrolyte Transport Properties and Limiting Currents with In Situ MRI Mapping of Lithium-Ion Battery Electrolyte Transport Properties and Limiting Currents with In Situ MRI. *J. Electrochem. Soc.* **2020**, *167*, 140518.

(18) Fawdon, J.; Ihli, J.; Mantia, F. L.; Pasta, M. Characterising lithium-ion electrolytes via operando Raman microspectroscopy. *Nat. Commun.* **2021**, 13–15.

(19) Wang, A. A.; Gunnarsdóttir, A. B.; Fawdon, J.; Pasta, M.; Grey, C. P.; Monroe, C. W. Potentiometric MRI of a Superconcentrated Lithium Electrolyte: Testing the Irreversible Thermodynamics Approach. *ACS Energy Lett.* **2021**, 3086–3095.

(20) Rey, I.; Bruneel, J.-L.; Grondin, J.; Servant, L.; Lassègues, J.-C. Raman Spectroelectrochemistry of a Lithium/Polymer Electrolyte Symmetric Cell. *J. Electrochem. Soc.* **1998**, *145*, 3034.

(21) Huang, Q.; Lee, Y. Y.; Gurkan, B. Pyrrolidinium Ionic Liquid Electrolyte with Bis(trifluoromethylsulfonyl)imide and Bis(fluorosulfonyl)imide Anions: Lithium Solvation and Mobility, and Performance in Lithium Metal-Lithium Iron Phosphate Batteries. *Ind. Eng. Chem. Res.* **2019**, *58*, 22587–22597.

(22) Umebayashi, Y.; Hamano, H.; Seki, S.; Minofar, B.; Fujii, K.; Hayamizu, K.; Tsuzuki, S.; Kameda, Y.; Kohara, S.; Watanabe, M. Liquid structure of and Li+ ion solvation in bis(trifluoromethanesulfonyl)amide based ionic liquids composed of 1-ethyl-3-methylimidazolium and N -methyl- N -propylpyrrolidinium cations. *J. Phys. Chem. B* **2011**, *115*, 12179–12191.

(23) Fujii, K.; Hamano, H.; Doi, H.; Song, X.; Tsuzuki, S.; Hayamizu, K.; Seki, S.; Kameda, Y.; Dokko, K.; Watanabe, M.; Umebayashi, Y. Unusual Li [+] Ion Solvation Structure in Bis(fluorosulfonyl)amide Based Ionic Liquid. *J. Phys. Chem. C* **2013**, *117*, 19314–19324.

(24) Liu, J.; Monroe, C. W. Solute-volume effects in electrolyte transport. *Electrochim. Acta* **2014**, *135*, 447–460.

(25) Aguilera, L.; Völkner, J.; Labrador, A.; Matic, A. The effect of lithium salt doping on the nanostructure of ionic liquids. *Phys. Chem. Chem. Phys.* **2015**, *17*, 27082–27087.

(26) Judeinstein, P.; Zeghal, M.; Constantin, D.; Iojoiu, C.; Coasne, B. Interplay of structure and dynamics in Lithium/Ionic liquid electrolytes: Experiment and molecular simulation. *J. Phys. Chem. B* **2021**, *125*, 1618–1631.

(27) Russina, O.; Lo Celso, F.; Di Michiel, M.; Passerini, S.; Appetecchi, G. B.; Castiglione, F.; Mele, A.; Caminiti, R.; Triolo, A. Mesoscopic structural organization in triphilic room temperature ionic liquids. *Faraday Discuss.* **2013**, *167*, 499–513.

(28) Pontoni, D.; Haddad, J.; Di Michiel, M.; Deutsch, M. Self-segregated nanostructure in room temperature ionic liquids. *Soft Matter* **2017**, *13*, 6947–6955.

(29) Hayes, R.; Warr, G. G.; Atkin, R. Structure and Nanostructure in Ionic Liquids. *Chem. Rev.* **2015**, *115*, 6357–6426.

(30) Castiglione, F.; Famulari, A.; Raos, G.; Meille, S. V.; Mele, A.; Appetecchi, G. B.; Passerini, S. Pyrrolidinium-based ionic liquids doped with lithium salts: How does Li+ coordination affect its diffusivity? *J. Phys. Chem. B* **2014**, *118*, 13679–13688.

(31) Lamb, H. *Hydrodynamics*, 4th ed.; Cambridge University Press, 1916.

(32) Castriota, M.; Caruso, T.; Agostino, R. G.; Cazzanelli, E.; Henderson, W. A.; Passerini, S. Raman investigation of the ionic liquid N-methyl-N-propylpyrrolidinium bis(trifluoromethanesulfonyl)imide and its mixture with LiN(SO 2CF3)2. *J. Phys. Chem. A* **2005**, *109*, 92–96.

(33) McEldrew, M.; Goodwin, Z. A.; Bi, S.; Bazant, M. Z.; Kornyshev, A. A. Theory of ion aggregation and gelation in super-concentrated electrolytes. *J. Chem. Phys.* **2020**, *152*, 1–19.

(34) Bard, A. J.; Faulkner, L. R. *Electrochemical Methods*, 2nd ed.; Wiley & Sons, 2001.

(35) Newman, J.; Thomas-Alyea, K. E. *Electrochemical Systems*, 3rd ed.; Wiley & Sons, 2004.

(36) Richter, J.; Amkreutz, E. On the Migration of Ions in Alkali Nitrate-Silver Nitrate Melts. *Zeitschrift fur Naturforsch. - Sect. A J. Phys. Sci.* **1972**, *27*, 280–287.

(37) Richter, J.; Gasseling, U.; Conradt, R. Transport numbers and ionic mobilities in nitrate melts by EMF-measurements on concentration cells with transference. *Electrochim. Acta* **1978**, *23*, 1165–1172.

(38) Hussey, C. L.; Sanders, J. R. Aluminum Bromide-1-Methyl-3-Ethylimidazolium Bromide Ionic Liquids:. *J. Electrochem. Soc.* **1987**, *134*, 1977.

(39) Ratkje, S. K.; Rajabu, H.; Førland, T. Transference coefficients and transference numbers in salt mixtures relevant for the aluminium electrolysis. *Electrochim. Acta* **1993**, *38*, 415–423.

(40) Haase, R. Internal and External Transport Numbers in Ionic Melts. *Zeitschrift fur Phys. Chemie* **1991**, *87*, 77–87.

(41) Doyle, M.; Fuller, T. F.; Newman, J. The importance of the lithium ion transference number in lithium/polymer cells. *Electrochim. Acta* **1994**, *39*, 2073–2081.

(42) Richter, J.; Sehm, S. Thermodynamic properties of Alkali Nitrate-Silver Nitrate Melts. *J. Phys. F Met. Phys.* **1972**, *2*, 833–841.

(43) Matsumoto, H.; Sakaebe, H.; Tatsumi, K.; Kikuta, M.; Ishiko, E.; Kono, M. Fast cycling of Li/LiCoO2 cell with low-viscosity ionic liquids based on bis(fluorosulfonyl)imide [FSI]-. *J. Power Sources* **2006**, *160*, 1308–1313.

(44) Bayley, P. M.; Best, A. S.; MacFarlane, D. R.; Forsyth, M. Transport properties and phase behaviour in binary and ternary ionic liquid electrolyte systems of interest in lithium batteries. *ChemPhysChem* **2011**, *12*, 823–827.